Impact of Humans on the Flux of Terrestrial Sediment to the Global Coastal Ocean

James P. M. Syvitski,[1]* Charles J. Vörösmarty,[2] Albert J. Kettner,[1,3] Pamela Green[2]

Here we provide global estimates of the seasonal flux of sediment, on a river-by-river basis, under modern and prehuman conditions. Humans have simultaneously increased the sediment transport by global rivers through soil erosion (by 2.3 ± 0.6 billion metric tons per year), yet reduced the flux of sediment reaching the world's coasts (by 1.4 ± 0.3 billion metric tons per year) because of retention within reservoirs. Over 100 billion metric tons of sediment and 1 to 3 billion metric tons of carbon are now sequestered in reservoirs constructed largely within the past 50 years. African and Asian rivers carry a greatly reduced sediment load; Indonesian rivers deliver much more sediment to coastal areas.

Coastal retreat has major implications for human habitat, because >37% (2.1 billion people in 1994) of the world's population live within 100 km of a coastline, and approximately 44% live within 150 km of a coastline (1). Coastal retreat is directly influenced by the reduction of river-supplied sediment (2). Thus, a goal of the International Geosphere Biosphere Programme (IGBP) and its core project, Land Ocean Interaction in the Coastal Zone (LOICZ), has been to survey the terrestrial sediment supply to the coast and to analyze human perturbation of this flux (3). Changes in sediment supply can greatly influence the benthic environment of coastal estuaries (4), coral reefs (5), and seagrass communities (6). In addition, nutrient fluxes, particularly carbon, are intimately tied to the flux of sediment (7), which has implications for coastal fisheries (8). Sediment delivery will also affect harbor maintenance and the potential for burial of pollutants (9).

Yet even with such environmental importance, <10% of the world's rivers have been monitored for their sediment delivery to the coastal zone or have observational data on them available to researchers (3). Of the rivers that have been monitored, most have had their sediment-gauging activities terminated (3). To address this paucity of data, we describe a globally consistent method for the estimation of the sediment flux near river mouths. We combine databases and models to determine the prehuman and modern delivery rate of sediment to the coast, including seasonal attributes, on a river-by-river global basis.

Global river discharge. A recent update to the Simulated Topological Network 30 minute (latitude × longitude) (STN-30p) for potential river flow paths (10) provides the spatial framework for organizing environmental data into distinct river basins. STN-30p is made up of ~60,000 grid cells at 30′ spatial resolution for the continental land mass. These cells define 6292 river basins with drainage areas >100 km². 4464 of these (i.e., those basins that are not covered by the ice sheets of Antarctica, Greenland, and portions of the Canadian Archipelago) have a positive discharge to the ocean or sea and are analyzed in this work. STN-30p catchment areas have a 7.5% absolute error, with a 2% positive bias (11).

The University of New Hampshire water balance and transport model (WBM/WTM), based on the STN-30p network, provides a fundamental structure for analyzing sediment flux distribution by river basin, continent, climatic zone, and receiving ocean or sea (12). WBM/WTM estimates of discharge are constrained by observed hydrographic data (11, 13). Selected (663) gauging stations from the Global Runoff Data Centre (GRDC) archive were coregistered to the STN-30p network, and these represent 76 Mkm² (72%) of the world's actively discharging landmass. The accuracy of GRDC discharge measurements is ~10 to 20%, which is much higher than what
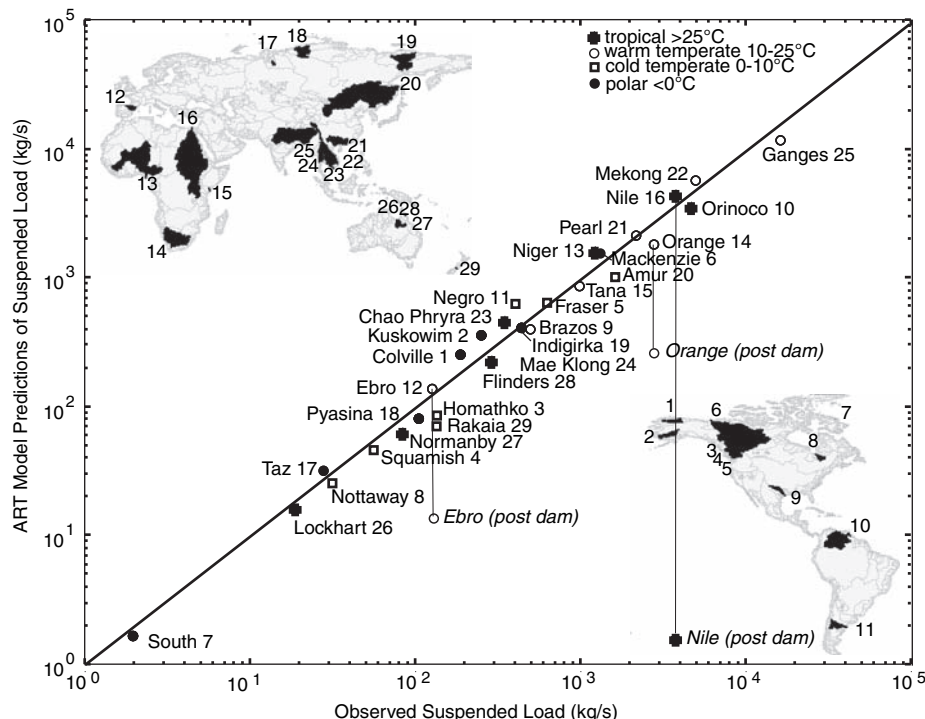
Fig. 1. Comparing observations of sediment loads with ART model predictions (16) for selected pristine (largely unregulated) rivers (e.g., South, Colville, Indigirka, Pyasina, Squamish, Kuskowim, Mae Klong, and Orinoco) or rivers observed before major human impacts (e.g., compare the after-dam values of the Ebro, Nile, and Orange with before-dam values). The data are from (16). The largest difference between predictions and observations is 63% (Negro). Errors associated with observational data are of the same magnitude as those associated with predictions.

[1]Environmental Computation and Imaging Facility, Institute of Arctic and Alpine Research (INSTAAR), University of Colorado, Boulder, CO 80309–0450, USA. [2]Water Systems Analysis Group, Institute for the Study of Earth, Oceans, and Space, University of New Hampshire, Durham, NH 03824, USA. [3]Applied Earth Sciences, Delft University of Technology, Delft, Netherlands.

*To whom correspondence should be addressed. E-mail: james.syvitski@colorado.edu

can be achieved from measuring precipitation (14). Differences between station data and simulated WBM/WTM discharge estimates derived from modern climatology were used to develop correction factors and then revised to account for human-induced losses of water within basins caused by interbasin water diversions or irrigation losses to the atmosphere. These factors are estimated to be 6% of the global discharge total of 40,000 km³/year (15). The resulting composite discharge field is a mix of observed discharge and WBM/WTM simulations where observations are not available, at a 0.5° × 0.5° resolution (latitude × longitude) for monthly climatology.

Global prehuman sediment flux. To predict the long-term fluvial discharge of sediment to the world's coastal zone, we used a drainage basin flux model (DBFM), which is based on relief, drainage area, or averaged discharge, and basin-distributed temperature (16). Unique solutions for each of the major climate regions (polar, temperate, and tropic) predict the flux of suspended sediment to within the uncertainties associated with global observations. Observational uncertainties can be large and may range from a factor of 2 for estimates for well-monitored rivers to an order of magnitude for poorly monitored rivers if important transport events are not captured (16, 17). Measured loads may also be biased if observations fall largely within a single climate period; variations in loads between wet and dry intervals of the Pacific/North American climate pattern may vary by a factor of 5 (18).

To determine the prehuman sediment load of global rivers, we used the Area Relief Temperature sediment delivery model (ART) version of the INSTAAR-DBFM model (12, 16). The use of the ART model as an estimator of prehuman global sediment loads is based on the following considerations. The model was trained on a global database of 340 rivers that cover 70% of the hydrologically active landmass, a majority of which are either in pristine form, or whose sediment loads were measured before the dominating impact of humans (before sediment sequestering in reservoirs, or increased sediment production from disturbance). Rivers in the database that showed large impact from human activities always fell off the line of regression between observation and prediction (16). On the basis of a smaller database of 145 major rivers (19), which were monitored across the 20th century, 48% of the rivers showed little change in their historical sediment loads, 47% showed decreasing loads caused by impoundments, and 5% showed increased sediment loads caused by disturbance. Walling and Fan (19) note that rivers showing little change in flux may "point to a lack of environmental change within the associated drainage basin, or at least a lack of sensitivity to ongoing changes, [or] … are buffered by the longer-term storage and remobilization of sediment within the upstream basin, associated with a relatively low sediment delivery ratio." Reductions could indicate deposition behind dams.

To test the appropriateness of using the ART model as an estimator of prehuman sediment flux, six to seven rivers from each climatic zone (polar, <0°C; cold temperate, 0° to 10°C; warm temperate, 10° to 25°C; and tropical, >25°C) were selected to be representative (small to large area, low to high relief)

Table 1. Predictions about the seasonal flux of sediment to the world's coastal zone under modern (Anthropocene) and prehuman conditions. Area, hydrologic-active drainage area with runoff >3 mm/year (global uncertainty ±7.5%) (11). Discharge, 35-year mean using the GRDC-WBM/WTM method of observations and predictions to determine composite runoff (global uncertainty ±15%) (14). Prehuman load Qs (sediment discharge), ART model predictions of fluvial long-term suspended sediment load (global uncertainty ±25%) (Fig. 1). Modern load Qs, observed suspended sediment loads where available (70% of global drainage) and QRT model predictions for the remaining 30% of world drainage, with sediment retention in large reservoirs taken into account (global uncertainty ±15%). Load retained in reservoirs, sediment flux trapped behind large reservoirs as percent of modern flux (uncertainties are ±30% of stated value). Trapping in small reservoirs increases by another 30% (global trapping of 20% would increase to 26% with small reservoirs). DJF, December January February; MAM, March April May; JJA, June July August; SON, September October November.

| | Area (Mkm²) | Discharge (km³/year) | Prehuman load Qs (MT/year) | Modern suspended sediment load Qs | | | | | Load retained in reservoirs |
| | | | | Annual (MT/year) | Seasonal percentages | | | | |
					DJF	MAM	JJA	SON	
Landmass									
Africa	20	3,800	1,310 ± 250	800 ± 100	30%	28%	22%	20%	25%
Asia	31	9,810	5,450 ± 1,300	4,740 ± 800	8%	12%	49%	31%	31%
Australasia	4	610	420 ± 100	390 ± 40	26%	27%	26%	21%	8%
Europe	10	2,680	920 ± 210	680 ± 90	29%	40%	18%	13%	12%
Indonesia	3	4,260	900 ± 340	1,630 ± 300	31%	28%	19%	21%	1%
North America	21	5,820	2,350 ± 610	1,910 ± 250	15%	24%	33%	28%	13%
Ocean islands	0.01	20	4 ± 1	8 ± 3	25%	13%	38%	25%	0%
South America	17	11,540	2,680 ± 690	2,450 ± 310	21%	32%	29%	18%	13%
Ocean basin									
Arctic Ocean	17	3,570	580 ± 120	420 ± 60	2%	20%	63%	15%	5%
Atlantic Ocean	42	18,480	3,850 ± 800	3,410 ± 420	20%	30%	27%	23%	14%
Indian Ocean	15	5,060	3,810 ± 1,020	3,290 ± 410	12%	12%	46%	30%	15%
Inland seas (endorheic)	5	400	470 ± 180	140 ± 30	13%	51%	28%	8%	30%
Mediterranean and Black Seas	8	710	890 ± 280	480 ± 60	43%	42%	9%	7%	30%
Pacific Ocean	18	10,320	4,430 ± 1,100	4,870 ± 910	18%	23%	33%	26%	26%
Climate zone									
Tropical (>25°C)	17	7,110	1,690 ± 480	2,220 ± 360	22%	17%	29%	32%	16%
Warm temperate (10–25°C)	47	21,110	9,070 ± 2,600	8,030 ± 1,250	18%	22%	35%	25%	15%
Cold temperate (0–10°C)	17	4,760	1,940 ± 250	1,460 ± 160	17%	35%	30%	19%	47%
Polar (<0°C)	24	5,560	1,330 ± 170	900 ± 120	2%	24%	58%	17%	6%
Elevation class									
High mountain (>5000 m)	21	12,500	5,120 ± 1,600	4,100 ± 740	11%	18%	44%	27%	31%
Mountain (3000–5000 m)	30	6,420	2,970 ± 610	2,190 ± 340	20%	28%	31%	21%	22%
Low mountain (1000–3000 m)	36	12,790	4,670 ± 1,030	4,800 ± 630	20%	23%	31%	25%	12%
Upland (500–1000 m)	10	3,670	910 ± 180	1,060 ± 110	24%	24%	28%	23%	4%
Lowland (100–500 m)	8	2,560	330 ± 70	360 ± 50	21%	34%	26%	19%	2%
Coastal plain (<100 m)	1	600	30 ± 10	100 ± 20	27%	40%	20%	13%	0%
Global	106	38,540	14,030	12,610	18%	23%	35%	25%	20%

and be either pristine (largely unregulated) or have observations collected before a major human disturbance (Fig. 1); for most rivers, the anthropogenic footprint increases sharply after World War II (*19*). The ART model shows no systematic bias and provides flux predictions within ±25% for these pristine or once-pristine rivers. Because the ART model, as applied here, does not take into account variability in geology, the model is not a good estimator everywhere. However, the ensemble regional estimates of landscape erosion before human influence should be reasonable.

Table 1 provides the prehuman fluxes of suspended sediment as differentiated by landmass, ocean basin or sea, climate zone, and elevation class. The global flux of sediment is 14 billion metric tons (BT, where 1 BT = 1 Tg) per year or, when a global estimate of bedload is included (*16*), 15.5 BT/year. Asia is the largest producer of fluvial sediment, followed by the Americas. The highest sediment yield (sediment load divided by drainage area) is from Indonesia and Oceania, both of which receive the most runoff (discharge divided by area). The lowest sediment yield is from the polar terrain draining into the Arctic Ocean. Warm temperate regions have the highest sediment yield as compared with other climates, and they account for nearly two-thirds of global sediment delivery. Close to 60% of global sediment delivery to the coastal zone is derived from basins draining high mountains (altitude >3000 m).

Global modern sediment flux. With the increase in human activities, much has changed in terms of sediment delivery, with variances in both directions (*19, 20*). Changes in surface runoff affect the transport agent of the fluvial load and include aquifer mining, surface water diversion, volume changes of inland lakes, desertification, wetland drainage, soil reservoir storage, deforestation, and dam building (*15*). Although these changes are almost in balance, with 200 km³ year⁻¹ in increased runoff balanced by water retention behind artificial impoundments of 170 km³ year⁻¹, the global pattern shows large regional differences (*15*). Reservoir operations also influence the timing of runoff; for example, there is winter release for hydroelectric power generation and summer release for agricultural purposes, in contrast with the more normal spring and fall wet periods in the temperate regions of the world. To address these contemporary issues, we used the GRDC–WBM/WTM composite discharge fields that define the modern Anthropocene world (that is, the period after the Industrial Revolution).

In addition to human impacts on global runoff, there are many anthropogenic influences on global sediment yield, including urbanization, deforestation, agricultural practices, mining, and the retention of sediment by reservoirs. These changes can affect both small river systems, where human activities can over-

whelm pristine conditions, and large systems such as the Mississippi, Colorado, Yellow, and Nile Rivers (*3, 19, 20*). The magnitude of the composite anthropogenic effect is a moving target. For example, historic land use and sediment discharge response have come full circle for the eastern seaboard of the United States, where peak fluxes occurred along with 18th-century deforestation but have returned to background conditions through reservoir construction (*21*).

To model the Anthropocene period, we merged observations (from the years 1960 to 1995) of sediment loads of rivers that drain 70% of the land surface and predictions from the Discharge Relief Temperature sediment delivery model (QRT) (*16*) for basins for which observations are missing (*12*). The QRT model is similar to the ART model in development, bias, and accuracy and also could be considered to represent pre-Anthropocene values. However, the QRT model uses discharge rather than basin area and is thus able to incorporate changes in runoff caused by humans. The QRT model also accounts for trapping of sediment in reservoirs (*22*). The load database includes observed values of sediment load both before and after damming (see Fig. 1 for reservoir influence on the Ebro, Orange, and Nile Rivers) and estimates of sediment trapping from both large and small reservoirs for the rivers ungauged for sediment flux (*22*).

Figure 2 shows the human impact on the natural sediment load estimates for 217 rivers with good observational data (before/after damming). When before-dam values are examined, the analysis indicates that the rivers are globally getting dirtier and would otherwise

move more sediment to the coast if not for the impact of reservoirs. Two curves excluding the impact of reservoirs are provided: one with and one without Yellow River (Huang He) loads. The Yellow is an example of a river whose sediment load is a moving target. In the period from 1950 to 1977, the Yellow River had a load of 1.6 BT/year, which was largely related to poor farming practices on the Loess Plateau (*23*). Since the 1980s, the sediment load of the Yellow has dropped to <50% of this earlier value because of a reduced hinterland precipitation, increased water abstraction, and improved sediment control practices in the Loess region (*19*). Other curves in Fig. 2 show the impact of sediment impoundment behind reservoirs. One curve demonstrates the basin-wide trapping of suspended sediment flux by the large (> 0.5 km³ maximum storage) reservoirs that account for about 70% of the impoundment storage volume filed with the International Commission on World Registry of Dams (*22*). Another curve highlights the impact of the millions of smaller reservoirs that have much lower trapping efficiencies because of their size but still greatly decrease the flux of sediment to the coast because of their number.

The global modern sediment flux is calculated to be 12.6 BT/year, or 10% less than the pre-Anthropocene load (Table 1). Given that large reservoirs trap 20% of the global sediment flux and small reservoirs trap another 6% (Table 1), then in a modern world without reservoirs, the global annual flux would be [(0.26 × 14 BT) + 12.6 BT] = 16.2 BT of suspended sediment, or 17.8 BT when bedload is included. This value is smaller than the 20 BT/year estimated by Milliman and Syvitski
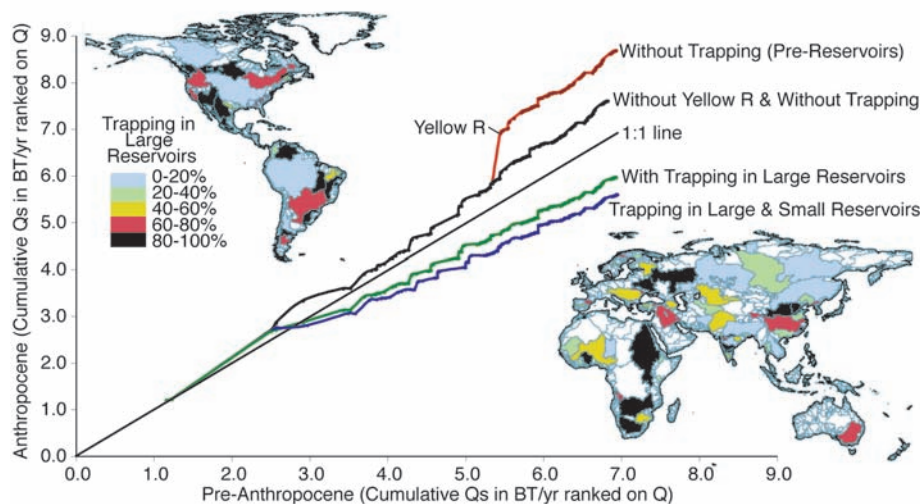
Fig. 2. Comparison between pre-Anthropocene (Fig. 1) and modern sediment loads, using 217 global rivers with good observational before- and after-dam data. Data are presented as cumulative curves ranked by decreasing river discharge (e.g., the first value to the left is the Amazon). 1:1 line represents no influence by humans. Two curves (with and without the Yellow River) had trapping by reservoirs removed and represent the increased sediment yield caused by human activity (e.g., deforestation). Two other curves show the impact of sediment sequestering in large or small reservoirs. Inserts include the global geography of basinwide trapping of sediment by large reservoirs (*22*).

(23), who surveyed a larger landmass in their analysis (the glaciated Arctic) and did not undertake a basin-by-basin upscaling analysis.

Africa and Asia see the largest reduction in sediment flux to the coast (Table 1 and Fig. 3) in rivers such as the Nile, Orange, Niger, and Zambezi in Africa and the Yangtze, Indus, and Yellow in Asia. Inland seas and the Mediterranean and the Black Seas, are the bodies of water most affected by reservoirs (Table 1) (2). The cold temperate zone encompasses the industrialized countries, where power consumption is highest, and host reservoirs that trap 47% of the regional sediment flux. As expected, mountain-draining rivers show decreased sediment fluxes on average, caused by the proliferation of impoundments (Table 1), in contrast to nonmountainous drainage basins, where sediment flux has increased (Table 1 and Fig. 3) (24). The tropics in general, and Indonesia in particular, are the regions most influenced by increased sediment loads (Table 1 and Fig. 3), largely because of deforestation (25).

Global modern seasonal sediment flux. To predict sediment discharge at the dynamic (daily) level, Morehead *et al.* (17) recast the classic rating curve to account for interday and interannual variability. Their PSI model successfully captures the behavior of both large and small rivers, such as the ice-melt–dominated Kliniklini River, British Columbia, Canada (26); the snowmelt Liard River, northern Canada (27); the rain-dominated Eel River, California, USA (28); the cyclone-dominated Lanyang River, Taiwan (29); and the agricultural Po River, Italy (30).

To apply the PSI model (12) to global rivers, we use the Anthropocene values of monthly discharge from the GRDC–WBM/WTM time series (1960 to 1995) and the merged observations/QRT simulations of long-term sediment load (Fig. 3). Figure 4 shows details of the result when applied to three river types. Monthly averages of the modeled discharge compare well with measured values and lie within the observed interannual variability. The Po is an exception and highlights the coarseness of the STN-30p grid, which is not able to separate two adjoining river basins (the Po and the Adige) (Fig. 4A, note 1). As a consequence, the modeled discharge is larger than observations for the Po alone. Modeled monthly averages of suspended load compare well for many rivers (e.g., the Fraser) (Fig. 4, center row) but show deviations for strongly influenced rivers. For example: (i) For the Mississippi, the modeled load is overpredicted
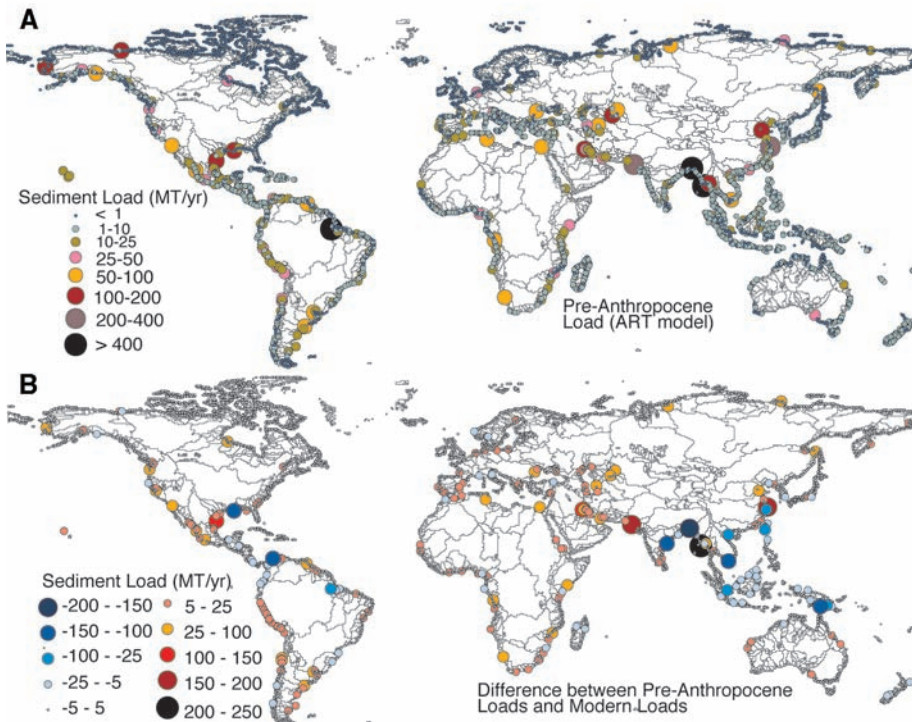
Fig. 3. (A) Global distribution of prehuman sediment flux, based on ART model (12) predictions (Fig. 1). **(B)** Differences between prehuman and modern sediment load [observations merged with QRT model predictions (12) accounting for anthropogenic impacts (22)] (Fig. 2).

Fig. 4. Observed and modeled monthly discharge and sediment load for three river types that highlight model capabilities and problems (see text for discussion of notes). The horizontal panels represent three rivers: (Top) The 3,220,000 km² Mississippi, USA; (middle) the 220,000 km² Fraser, Canada; (bottom) the 77,000 km² Po, Italy. **(A)** Observed water discharge with 35-year mean ± 1 SD and the composite WBTM discharge values (12). **(B)** Observed sediment discharge with 35-year mean ± 1 SD and QRT-PSI model predictions (12). **(C)** Time series of observed monthly sediment load and QRT-PSI predictions (12).
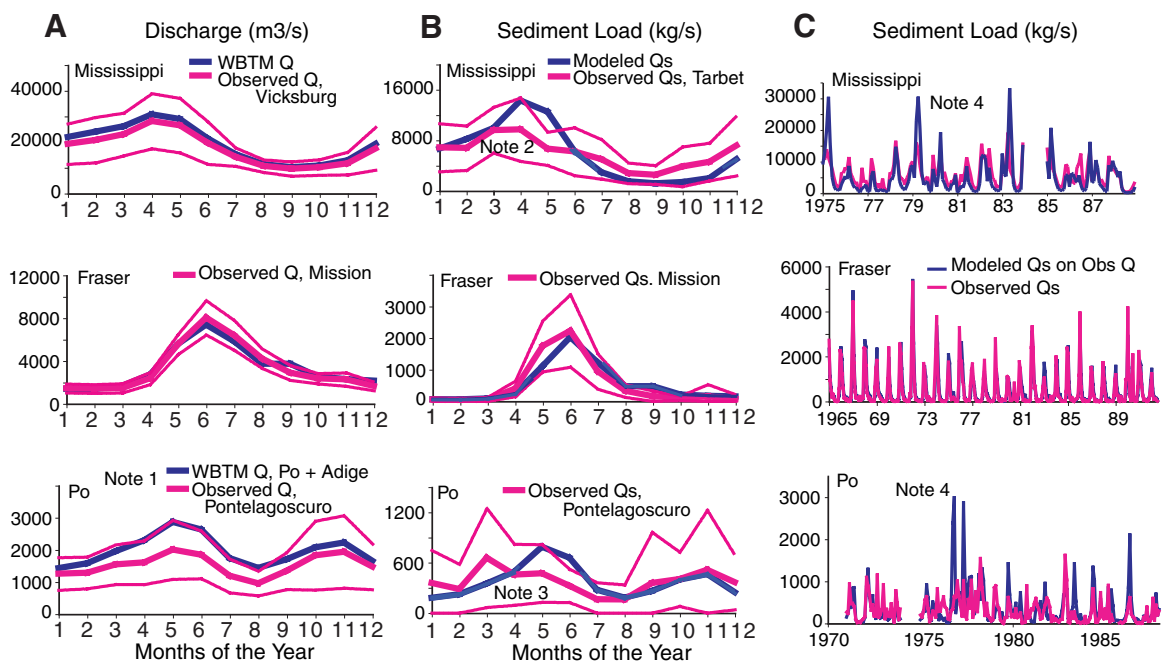
in the spring and underpredicted in the fall, because the full impact of the basin's 65,000 reservoirs is not adequately captured (Fig. 4B, note 2). (ii) For the Po, the modeled load does not capture the two-dimensional effect of different water sources (for example, relatively clean water released from large Alpine reservoirs during winter months compared with the unfiltered Apennine load) (Fig. 4B, note 3). These variances are clearly seen on the time series of sediment discharge (Fig. 4C, note 4). Seasonal averages were therefore calculated to reduce these within-month variances.

To calculate the global seasonal sediment load, we applied the composite observation/WBM/WTM-QRT PSI model to produce global monthly averages of sediment loads (12). The monthly values are summed across March to May, June to August, September to November, and December to February, in order to produce the seasonal values (Table 1 and Fig. 5). The influence of the geographic asymmetry of the world's landmass is amplified by the patterns of the monsoonal discharge (i.e., December to April in the southern tropics versus June to October in the northern tropics), temperate discharge (winter/spring rain and snowmelt), and arctic discharge (summer rain mixed with snow and ice melt) (Fig. 5). Table 1 shows which coasts are dominated by highly seasonal fluxes of sediment and which receive more constant, albeit episodic, fluxes of material. Rivers affected by monsoons are highly seasonal in their sediment fluxes (e.g., in Indonesia and Asia).

Figure 5 also depicts the east coast of the Americas, where flux patterns show similarity to global seasonal patterns but also deviations that reflect the size distribution of drainage basins relative to mountain chains and climate zones. As expected, the Arctic Ocean, polar region, and rivers draining high mountains show the largest seasonality in their sediment flux (Table 1).

Summary. This study attempts to predict the global flux of sediment on a river-by-river basis (4462 rivers >100 km^2) under modern conditions and before human influence. The method allows global hot spots to be located on a 0.5° grid of the global coast. These hot spots of high or modified sediment flux should allow coupled, dynamic, ocean-land-atmosphere models to be developed. Humans are simultaneously increasing the river transport of sediment through soil erosion activities and decreasing this flux to the coastal zone through sediment retention in reservoirs. The net result is a global reduction in sediment flux by about 1.4 BT/year over prehuman loads. This impact on coastal erosion will be further accelerated as the sea level rises, which is anticipated because of human-induced climate change (31). Given the modern levels of fluvial sediment loads, over 100 BT of sediment, including carbon (~1 to 3%), have been sequestered behind human-made reservoirs. Regions with more limited reservoir construction, such as Indonesia, see much of the sediment production and transported carbon buried on the surrounding continental margins. The seasonal pattern in the global delivery of sediment to the coast is displayed here and should be a valuable aid to those investigating the dynamics of nutrient fluxes to the coast and to those monitoring coastal fisheries, coral reefs, and seagrass communities.

References and Notes
1. J. E. Cohen *et al.*, *Science* **278**, 1209 (1997).
2. C. Liquete, M. Canals, P. Arnau, R. Urgeles, X. Durrieu de Madron, *Oceanography* **17**, 70 (2004).
3. J. P. M. Syvitski, *Global Planet. Change* **39**, 1 (2003).
4. E. Wolanski, S. Spagnol, *Reg. Environ. Change* **1**, 152 (2000).
5. C. J. McLaughlin, C. A. Smith, R. W. Buddemeier, J. D. Bartley, B. A. Maxwell, *Global Planet. Change* **39**, 191 (2003).
6. J. D. Restrepo, P. Zapata, J. M. Diaz, J. Garzon-Ferreira, C. B. Garcia, *Global Planet. Change*, in press.
7. S. V. Smith, W. H. Renwick, R. W. Buddemeier, C. J. Crossland, *Global Biogeochem. Cycles* **15**, 697 (2001).
8. G. Marmulla, Ed., *Dams, Fish and Fisheries, Opportunities, Challenges and Conflict Resolution. FAO Fisheries Tech. Paper 419* [Food and Agriculture Organization (FAO) of the United Nations, Rome, 2001].
9. J. P. M. Syvitski, D. C. Burrell, J. M. Skei, *Fjords: Processes & Products* (Springer, New York, 1987).
10. C. J. Vörösmarty, B. M. Fekete, M. Meybeck, R. Lammers, *Global Biogeochem. Cycles* **14**, 599 (2000).
11. B. M. Fekete, C. J. Vörösmarty, W. Grabs, *Global, Composite Runoff Fields Based on Observed River Discharge and Simulated Water Balances* (Report No. 22, GRDC, Koblenz, Germany, ed. 2, 1999).
12. Materials and methods are available as supporting material on *Science* Online.
13. The World Meteorological Organization GRDC archive is available online at http://grdc.bafg.de.
14. S. Hagemann, L. Dümenil, *Clim. Dyn.* **14**, 17 (1998).
15. C. J. Vörösmarty, D. Sahagian, *Bioscience* **50**, 753 (2000).
16. J. P. M. Syvitski, S. D. Peckham, R. D. Hilberman, T. Mulder, *Sediment. Geol.* **162**, 5 (2003), and erratum, *Sediment. Geol.* **164**, 345 (2004).
17. M. D. Morehead, J. P. M. Syvitski, E. W. H. Hutton, S. D. Peckham, *Global Planet. Change* **39**, 95 (2003).
18. D. L. Inman, S. A. Jenkins, *J. Geol.* **107**, 251 (1999).
19. D. E. Walling, D. Fan, *Global Planet. Change* **39**, 111 (2003).
20. J. A. Dearing, R. T. Jones, *Global Planet. Change* **39**, 147 (2003).
21. G. B. Pasternak, G. S. Brush, W. B. Hilgartner, *Earth Surf. Processes Landforms* **26**, 409 (2001).
22. C. J. Vorosmarty *et al.*, *Global Planet. Change* **39**, 169 (2003).
23. J. D. Milliman, J. P. M. Syvitski, *J. Geol.* **100**, 525 (1992).
24. I. Douglas, in *The Earth as Transformed by Human Action*, B. L. Turner *et al.*, Eds. (Cambridge Univ. Press, Cambridge, 1993), pp. 215–234.
25. D. Hu, Y. Saito, S. Kempe, in *Asian Change in the Context of Global Climate Change: Impact of Natural and Anthropogenic Changes in Asia on Global Biogeochemical Cycles*, J. N. Galloway, J. M. Melillo, Eds. (IGBP Publication Series 3, Cambridge Univ. Press, Cambridge, 2001), pp. 245–270.
26. M. D. Morehead, J. P. M. Syvitski, E. W. H. Hutton, *Global Planet. Change* **28**, 107 (2001).
27. J. P. M. Syvitski, *Polar Res.* **21**, 323 (2002).
28. J. P. M. Syvitski, M. D. Morehead, *Mar. Geol.* **154**, 13 (1999).
29. J. P. M. Syvitski, A. J. Kettner, S. D. Peckham, S.-J. Kao, *J. Coastal Res.*, in press.
30. J. P. M. Syvitski, A. J. Kettner, A. Correggiari, B. W. Nelson, *Mar. Geol.*, in press.
31. J. P. M. Syvitski *et al.*, *LOICZ: Coastal Change and the Anthopocene*, C. Crossland, Ed. (Springer, New York, in press).
32. We thank the Office of Naval Research and NASA (IDS/NNG04GH75G) for financially supporting this investigation and IGBP, LOICZ, and Global Water System Project scientists for supporting workshops and discussions that led to this analysis.
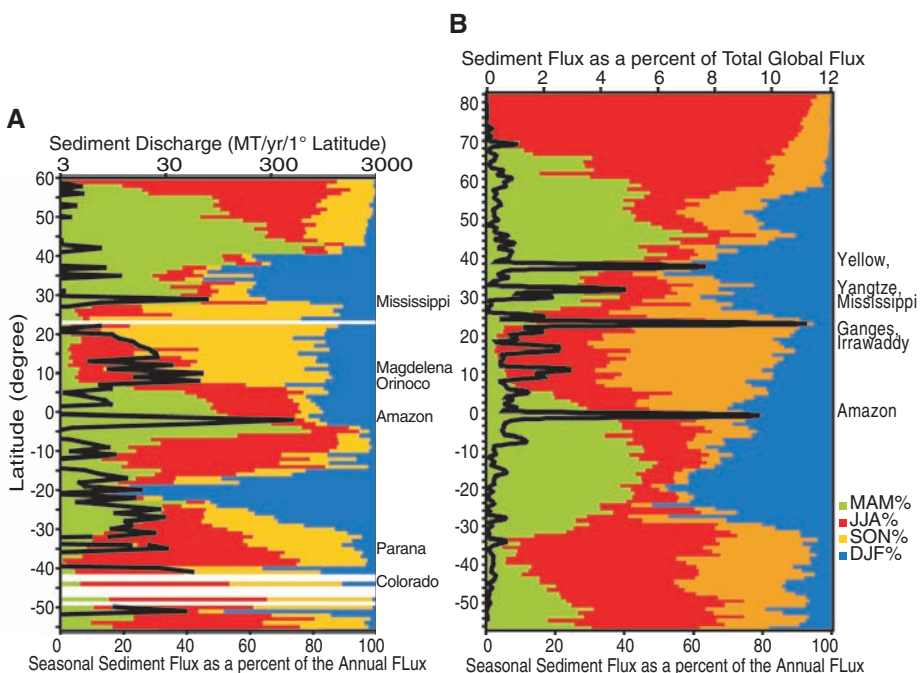
Fig. 5. Modern seasonal sediment load for global rivers. (**A**) Seasonal flux as percent of annual flux for rivers draining from the Americas into the Atlantic Ocean. Green, MAM; Red, JJA; Yellow, SON; Blue, DJF. Superimposed is the annual flux averaged across 1° of latitude, with major rivers that contribute to hot spots of sediment discharge. (**B**) Seasonal flux to the world's coastal zone, as percent of annual flux. Superimposed is the annual flux as percent of global total, averaged across 1° of latitude, with major rivers that contribute to hot spots of sediment discharge.